Polypyrrole/Silver Coaxial Nanowire Aero-Sponges for Temperature-Independent Stress Sensing and Stress-Triggered Joule Heating

Weina He,[†] Guangyong Li,[†,§] Shangquan Zhang,[†] Yong Wei,[†,§] Jin Wang,[†] Qingwen Li,[†] and Xuetong Zhang*[,†,‡]

[†]Suzhou Institute of Nano-tech & Nano-bionics, Chinese Academy of Sciences, Suzhou, Jiangsu 215123, P. R. China, [§]Department of Chemistry, College of Sciences, Shanghai University, Shanghai 200444, P. R. China, and [‡]School of Materials Science & Engineering, Beijing Institute of Technology, Beijing 100081, P. R. China

ABSTRACT To obtain ideal sensing materials with nearly zero temperature coefficient resistance (TCR) for self-temperature-compensated pressure sensors, we proposed an Incipient Network Conformal Growth (INCG) technology to prepare hybrid and elastic porous materials: the nanoparticles (NPs) are first dispersed in solvent to form an incipient network, another component is then introduced to coat the incipient network conformally *via* wet chemical route. The conformal coatings not only endow NPs with high stability but also offer them additional structural elasticity, meeting requirements for future generations of portable, compressive and flexible devices. The resultant polypyrrole/silver coaxial nanowire hybrid aero-sponges prepared *via* INCG technology have been processed into a piezoresistive sensor with highly sensing stability (low TCR 0.86 × 10^{-3}/°C), sensitivity (0.33 kPa^{-1}), short response time (1 ms), minimum detectable pressure (4.93 Pa) after suffering repeated stimuli, temperature change and electric heating. Moreover, a stress-triggered Joule heater can be also fabricated mainly by the PPy-Ag NW hybrid aero-sponges with nearly zero temperature coefficient.

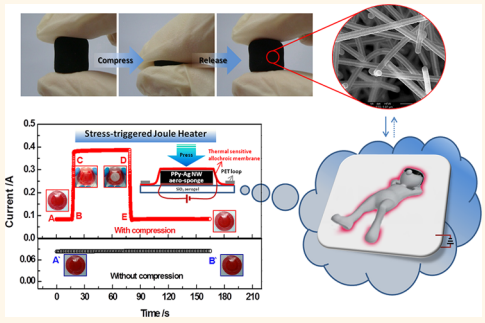

KEYWORDS: hybrid sponge · nearly zero temperature coefficient resistance · self-temperature compensation · stress sensor · Joule heater

Hybrid materials are becoming increasingly important because of the possibility to benefit from the best of organic and inorganic realms. They are considered as an attractive, versatile, technological platform for future electronic, optical, magnetic, and energetic applications.[1−8] Even so, numerous of research works mainly focus on the combined advantages of each component, having not paid much attention to offsetting the weaknesses of nanocomponents. However, the selectively offsetting becomes crucial for some special applications, such as sensing. The irrelevant influencing factors on sensing materials can be picked off upon a deliberate positioning of the building blocks with opposite dependence upon external stimuli.[9]

Piezoresistive sensors, transducing pressure message to resistance signal, have been rapidly developed and widely used for their advantages in high sensitivity, fast response, feasible fabrication, low cost, and easy signal collection.[9−19] However, as the core part of sensors, the piezoresistive materials always show temperature drift caused by the temperature-dependent electrical resistances. So, the temperature compensation has to be involved in order to determine the stress being measured accurately.[20−24] Even so, the temperature compensation systems have to be calibrated frequently due to the newly exploit and volatile application environments, making the measurements more complex and applicably restricted. Hence, self-temperature-compensated sensors are highly desirable in direct and precise measurement. The most feasible solution is developing hybrid sensing materials with a low/nearly zero temperature coefficient resistivity (TCR) by

* Address correspondence to zhangxtchina@yahoo.com.

Received for review January 28, 2015 and accepted March 26, 2015.

Published online March 26, 2015
10.1021/acsnano.5b00626

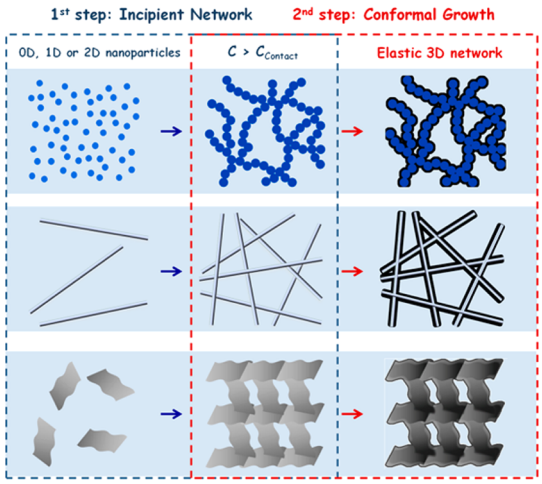

Figure 1. Schematic representation of how the Incipient Network Conformal Growth (INCG) technology operates.

offsetting the positive and negative temperature-dependence of electric resistance.

Conductive and elastic sponges are an emerging kind of candidates for fabrication of piezoresistive sensors because of their combinational electric conductivities and mechanical flexibilities. Heretofore, conductive sponges are mainly obtained from (a) metal aerogel produced by sol−gel procedure,[25−30] (b) carbonized product of organic aerogel,[31−34] and (c) nanomaterial self-assembled by CNTs or G/GO sheets.[35−49] However, few of them exhibit a low/nearly zero temperature coefficient resistivity (TCR) with a single component.

Therefore, we proposed an Incipient Network Conformal Growth (INCG) technology to prepare hybrid and elastic porous materials. A polypyrrole/silver (PPy/Ag) coaxial nanowire hybrid aero-sponge (we called the resultant porous material "aero-sponge" because it was prepared *via* wet chemical and supercritical drying procedure analogous to "aerogel") was prepared successfully *via* INCG technology in a programmable way. Through the wise selection of the ratio of PPy to Ag, the electric resistance of the hybrid aero-sponges can be immune from temperature influence. The resultant aero-sponges are ideal candidates for stress-sensing and Joule-heating materials with nearly zero temperature coefficient behaviors.

RESULTS AND DISCUSSION

We proposed an Incipient Network Conformal Growth (INCG) technology to prepare hybrid and elastic porous materials (Figure 1). 0D, 1D or 2D nanoparticles (NPs) are first dispersed in solvent to form a uniform suspension. Once the suspension is within a proper concentration range, the incipient network will be formed *via* NPs contact with each other. Another component is then introduced and supposed to coating the incipient network conformally. The conformal coatings not only endow NPs with high

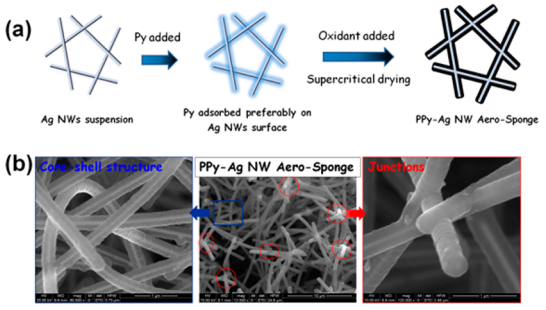

Figure 2. Schematic representation of the formation of PPy-Ag NW aero-sponges. (a) Schematic illustration for the fabrication process of PPy-Ag NW aero-sponges. (b) SEM images of Ag NW-PPy aero-sponges with red circles highlighting the *in situ* welded junctions and enlargements of structural details.

stability but also offer them additional structural elasticity, meeting requirements for future generations of portable, compressive and flexible devices.

Ag nanowires (Ag NWs) were herein selected to build the incipient 3D networks because of its mature synthesis route and uniform diameters. The morphology of the obtained Ag NWs was investigated by Scanning Electron Microscope (SEM) measurements. From the SEM results (Supporting Information Figure S1), we can see that Ag NWs show uniform diameter of about 50 nm and length of tens of micrometers. Doi and Edwards theory was adopted to evaluate the solution range of Ag NWs suspension, regarding Ag NWs as rod-like molecules.[50,51] The Ag NWs concentration described through the volume fraction φ is defined as

$$\phi = \frac{\pi n L d^2}{4} = \frac{\pi n L^3}{4r^2}$$

where n is the number of Ag NWs per unit volume, while L, d, and r are the length, diameter, and a corresponding aspect ratio ($r = L/d$) of each Ag NW, respectively. According to the theory, once the concentration of the Ag NWs suspension reaches $\varphi_1 = \pi/(4*r^2)$, *i.e.*, $n = 1/L^3$, Ag NWs begin to contact with each other, while at a higher concentration of $\varphi_2 = 1/r$, *i.e.*, $n = 1/(dL^2)$, the nanowire suspension forms a 3D continuous network due to the physical bonds formation between nanowires. That is to say, Ag NWs suspension with the volume friction between $\varphi_1 = 8 \times 10^{-7}$ and $\varphi_2 = 10^{-3}$ was appropriate in this work to form an incipient 3D networks, taken $L \approx 50\ \mu$m and $d \approx 50$ nm for calculation.

Pyrrole (Py) was chosen to coating Ag NW to form elastic and conductive aero-sponges. The fabrication process for PPy-Ag NW hybrid aero-sponge is demonstrated in Figure 2a. Above the critical concentration of $\varphi_1 = 8 \times 10^{-7}$, the dispersed Ag NWs in suspension were intercontacted to build a 3D network at first. Py was then added into the suspension and the core−shell structure was formed resulting from metal-π

strong interactions. Once the oxidant was introduced, Py was oxidized and polymerized *in situ*. Thus, the 3D network and the core−shell morphology were fixed. After 24 h aging and 7 days solvent exchange by water and ethanol sequentially, the PPy-Ag NW hydrogels were converted into aero-sponges by supercritical CO_2 drying process.

It can be confirmed from the SEM images (Figure 2b) that the 3D network has been built by PPy-Ag NW coaxial wires with *in situ* welded junctions. The core−shell structure can be indicated by the brightness contrast in SEM images caused by the emission differences of secondary electrons for PPy and Ag NWs. The core−shell structure and PPy-Ag interface can be also clearly viewed from Transmission Electron Microscope (TEM) images (Supporting Information Figure S2). The easily recognized *in situ* welded junctions, highlighted by the red circles in Figure 2b, were formed by enwrapping of polymer onto contacted Ag NWs conformally. Raman and XRD measurements were also carried out to analyze the chain structure and regularity (Supporting Information Figures S3, S4). Compared with pure PPy, elaborate chemical bond deformations of PPy-Ag NW hybrid materials can be figured out from the Raman spectroscopy contributed by the Surface-Enhanced Raman Scattering (SERS) effect of Ag NWs.[52] Meanwhile, Ag NWs are confirmed maintaining superb crystallization attribute from XRD analysis. The bulk density of the resultant PPy-Ag NW hybrid aero-sponge can be adjustable within 9.2−203.7 mg/cm^3, controlled by the amount of Ag NWs and Pyrrole added. The bulk density of porous materials obtained *via* INCG technology can be adjusted in a wider range, compared with CNT (3−30 mg/cm^3) or G/GO (0.16−96 mg/cm^3) aerogels.[35−49]

As was expected, the synthesized PPy-Ag NW aero-sponges exhibited superb compressive elasticity. The aero-sponge could be compressed by large deformations (>90%) and recovered to its original shape in seconds (Figure 3a). As the compressive stress σ *versus* stain ε curves for the obtained aero-sponge along the loading direction during loading−unloading cycles shown, σ returns to the original values after unloading for each ε at 10−90% (Figure 3b). Although we found hysteresis loops in loading−unloading cycles, indicating dissipations, that did not affect the shape recovery of the obtained aero-sponges. From the comparison of the σ *vs* ε curves for 50 compress-release circles, the PPy-Ag NW aero-sponge can recover their original shape with little mechanical failure under fixed compression strain (Figure 3c).

The superb elasticity of the PPy-Ag NW aero-sponge is attributed to the particular network structures obtained *via* INCG technology. The resultant aero-sponges possess: (a) strength and flexible 3D network contributed by ultra-long coaxial nanowires, giving materials resistance to external compressions and

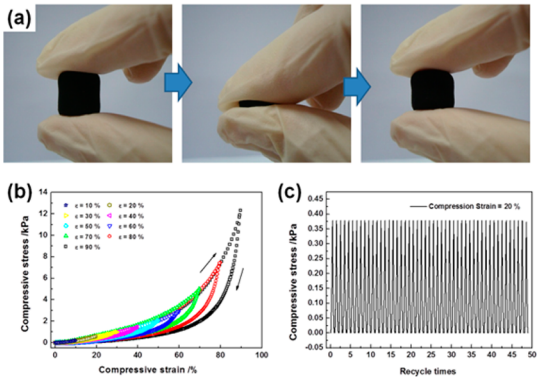

Figure 3. Elasticity of PPy-Ag NW aero-sponges. (a) Digital pictures, showing that hybrid aero-sponge recovers its original shape after it is compressed by large deformation. (b) σ *versus* ε curves for PPy-Ag NW aero-sponge along the loading direction during loading−unloading cycles at ε = 10−90%. (c) A total of 50 consecutive compression tests to the obtained PPy-Ag NW aero-sponge at 20% strain with little mechanical failure.

structural elasticity by bending the framework skeletons; (b) rich pores, providing the possibility of compressed aero-sponges to dissipate the external energy by shutting off the pores without breaking the gel frameworks; (c) *in situ* welded junctions and strong metal-π interactions, avoiding the interfacial slippage resulting from the poor load transfer between adjacent NPs or NPs and surrounding coatings.

On the basis of the specific structure of PPy-Ag NW aero-sponges, a programmed fabrication strategy could be also realized by regulating the synthesis conditions. First, the size and dispersity of pores in the network have been easily controlled by the concentration of the Ag nanowire solution (Supporting Information Figure S5). Second, the thickness of the skeleton could be regulated readily by modulating the ratio of Py to Ag NWs and reacting time. Increasing the relative Ag NWs content from 1.9 to 15.6 wt %, the PPy shell thickness was reduced from 375 to 125 nm (Figure 4a−c, Supporting Information Figure S6 and Table S1). If we neglect the effect of junctions to the core−shell structure, the PPy shell thickness could be theoretically estimated (Supporting Information Theoretical Analysis). There was a good corresponding relationship between experimental data and theoretical prediction (Figure 4d). In addition, the thickness of the PPy shell could be regulated by the reaction time (Supporting Information Figure S7). The INCG technology of preparing PPy-Ag NW hybrid aero-sponge reported here shows large superiority in programmable fabrication compared with other methods to obtain hybrid porous materials.[9,13,18]

In the next, we tried to clarify how the structures of PPy-Ag NW aero-sponges affect their properties. The electric conductivity of PPy-Ag NW aero-sponges are affected mainly by the junction density of the network, while the flexibility and strength of the frameworks are

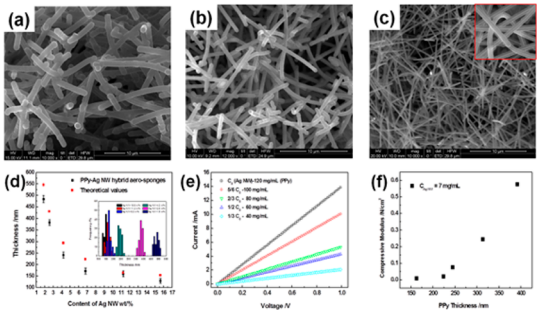

Figure 4. Programmed syntheses of PPy-Ag NW aero-sponges. (a−c) SEM images of PPy-Ag NW aero-sponge containing 1.9 (a), 4.2 (b), and 15.6 wt % (c) Ag NWs. (d) The relationship between Ag NWs content and PPy shell thickness (inset in (d) is the comparison of the shell thickness of various samples). (e) The comparison of current−voltage (*I*−*V*) curves. (f) Compressive modulus of hybrid aero-sponges with different junction densities and PPy shell thickness.

decided by the shell thickness directly. The junctions were formed randomly, which was decided by the INCG process. The incipient network was formed by the intercontact of nanoparticles dispersed in suspension and then fixed by the *in situ* conformal coating of conducting polymers. Because of the Brownian movement of the nanoparticles in suspension, the incipient network was dynamic and the junctions were formed randomly, which means that the precise control of junction density remains a big challenge. However, the density of the randomly formed junctions showed statistical regularity in large scale controlled by the concentration of nanoparticles suspension. To illustrate the influence of junction density on the electric conductivity of aero-sponges, we changed the concentration of Ag NWs and Py simultaneously to obtain the similar PPy shell thickness. It is revealed from the results (Figure 4e) that the denser the network, the higher electric conductivity. In the same way, fixing the concentration of the Ag NWs at about 7 mg/mL and increasing the Py concentration from 40 to 120 mg/mL, the compressive modulus of the hybrid aero-sponge increased with the PPy shell thickness (Figure 4f, Supporting Information Figure S5f and Table S2). In one word, due to the structural controllability and direct relationship of the properties and structures, PPy-Ag NW aero-sponges have been synthesized with designed structures and properties in a programmable way.

The synthesized PPy-Ag NW hybrid aero-sponge was expected to be an ideal sensing material for piezoresistive sensors for the following three reasons: (a) The hybrid aero-sponges possess rich pores and 3D flexible networks contributed by ultra-long nanowires, giving material better compressive elasticity and sensing sensitivity. (b) Owing to the highly adjustability of the structure and property, a series of PPy-Ag NW conductive aero-sponges can be prepared to meet the various application requirements in sensing sensitivity, pressure range and detection limit. (c) Most importantly, low temperature-coefficient stressing materials are more likely obtained from metal-conducting polymer hybrid aero-sponges.

Although conductive and elastic sponges are an emerging kind of candidates for fabrication of piezoresistive sensors, few of the existing conductive sponges (*e.g.*, polyurethane foam covered by conductive polymers or graphene sheets) serving as piezoresistive sensors showed low temperature coefficient of resistivity (TCRs), which of great importance in precise measurement.[9,13,15,18,53] Nevertheless, the low TCRs is possibly realized in PPy-Ag NW hybrid aero-sponge prepared *via* INCG technology reported here. Ag NWs experience an increase in electric resistance while their temperature is raised, named positive temperature-coefficient (PTC) property, while polypyrrole (PPy) showed negative temperature-coefficient (NTC) of electric resistance agreeing with Steinhart-Hart equation.[54,55] For the hybrid sponge of these two components, the temperature dependence of electric resistance can be probably tuned between the two components by changing their weight proportions.

For the hybrid aero-sponge of PPy and Ag NW, network was built mainly by the connection *via* Ag NWs cores (contributed by interconnected Ag NWs in suspension) or *via* PPy shells (resulting from the increased volume fiction of nanocables during the polymerizing procedure), illustrated in the insets of Figure 5a. The electric resistance changes of the hybrid aero-sponges are mainly influenced by PTC property of Ag NWs in the former connection mode, while the NTC property of PPy in the latter one. Then the temperature dependence of electric resistance can be regulated between the two components by changing their weight proportions. In a wide range, the higher of Ag NWs suspension initial concentration, the more direct contacting points between Ag NWs in 3D network and the less sensitive of the electric resistance to the temperature (Figure 5a, Supporting Information Figure S8). Increasing the Ag NWs concentration until its weight contention reached 83.3 wt %, a nearly zero temperature coefficient sample was obtained (Supporting Information Figure S9). Increasing the temperature from 17 to 50 °C, the relative change of the electric resistance was less than 3% (Figure 5a), and the TCR (= $(\Delta R/R_0)/\Delta T$) value of the hybrid aero-sponge was 0.86×10^{-3} /°C. To the best of our knowledge, few of the existing conductive sponges or films serving as piezoresistive sensors concerned about the resistance deviations with temperature, although it should not be neglected. Among the rare sensing materials concerned the resistance stability, the TCR of our aero-sponge in the general sensing temperature range (e.g., 15−50 °C) is the nearest to zero (exceeding 7×10^{-3} /°C of the ultrasensitive pressure sensor based on conducting polymer films reported by Zhenan Bao),[56] and is even already within the TCR range of standard

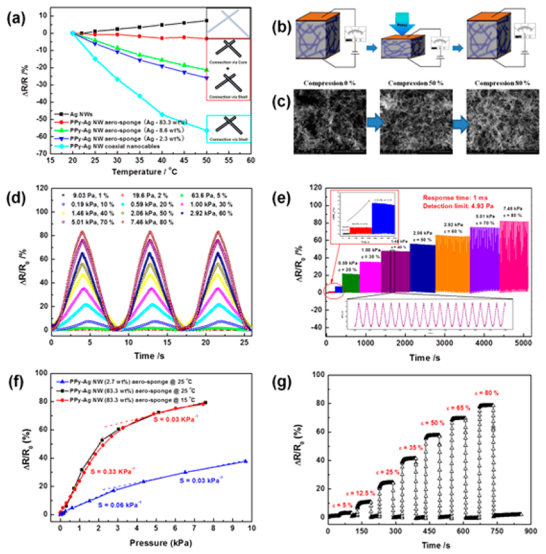

Figure 5. Properties of PPy-Ag NW hybrid aero-sponges in stress sensing. (a) The relative electric resistance changes−temperature ($\Delta R/R - T$) curves for Ag NWs, PPy-Ag NW membrane deposited by nanocable suspension, and PPy-Ag NW hybrid aero-sponge, respectively. (b) Schematic illustration of how to prepare a stress sensor with PPy-Ag NW aero-sponge, copper sheets, and metal wires. (c) SEM images of PPy-Ag NW aero-sponge with 0, 50, and 80% compression. (d) Multiple-cycles electric resistance tests of repeated loading and unloading pressure with different values with 1 V voltage input. (e) Reliability test of PPy-Ag NW hybrid aero-sponge under repeated loading and unloading pressure at different values with partial enlarged details in insets. (f) The relative electric resistance changes−compressive pressure ($\Delta R/R - p$) curves for PPy-Ag NW aero-sponge performed at 25 and 15 °C, respectively. (g) Electric resistance response of nearly zero temperature coefficient sensor at different strain by introducing a series of persistent compressive pressure.

resistors with low-resistance. The superb low TCR of the PPy-Ag NW hybrid aero-sponge means that it would be an ideal candidate for stress sensors.

To process into a stress sensor, the PPy-Ag NW aero-sponge was imbedded into two parallel copper electrodes and two copper wires were connected onto the electrodes, as shown in Figure 5b. Then, it was connected into an electric loop to detect the electric resistance changes ($\Delta R/R_0 = (R_0 - R)/R_0$, where R_0 and R denote the resistance without and with imposed stress, respectively) when it was compressed. SEM measurement was taken to observe the microscopic changes of the aero-sponge when suffering 0%, 50%, 80% compression (Figure 5c). The original aero-sponges exhibit many macro pores with diameters of about 10 μm. The more compressive pressure was imposed on the aero-sponge, the compacter the network showed with more contact numbers and lower electric resistance reasonably.

The electric resistance decreased directly with the compression strain, changing by 83% when it was compressed by 80% at most (Figure 5d). The electrical response speed and stability of the aero-sponge sensor were investigated by alternate supply of compressive and release stimuli. The electric resistance decrease of PPy-Ag NW aero-sponge caused by compression could be completed within 1 ms at least and so was the electric resistance recovery once the aero-sponge was released (Supporting Information Figure S10a), which is much shorter than the response time of SWNTs/PDMS film (<10 ms) and microstructured PPy thin film (~47 ms) reported elsewhere.[12,56] The minimum value of detectable pressure was as low as 4.93 Pa when the aero-sponge was compressed by 0.5% (Supporting Information Figure S10b), making our sensor more sensitive than the interlocking nanowire-type pressure sensor (5 Pa)[57] and graphene−polyurethane sponge based on fractured microstructure design (9 Pa).[13] Furthermore, the electrical response of PPy aero-sponge to the external stress stimuli exhibited high stability during hundreds of compression and release circles for each compressive strain (Figure 5e).

The sensitivity S (defined as $S = \delta(\Delta R/R_0)/\delta\sigma$) was as high as 0.33 kPa^{-1} for the nearly zero temperature coefficient sample, while S = 0.06 kPa^{-1} for another sample with a low Ag NW content of 2.7 wt % (Figure 5f). It implies that a series of sensing samples with different sensitivities can be prepared by programmed synthesis. To our best knowledge, the sensitivity of the nearly zero temperature-coefficient sample shows great superiority to other reported sponge-type piezoresistive sensors,[9,13,18] especially exceeding the highly pressure-sensitive graphene-polyurethane sponge based on fractured microstructure design (0.26 kPa^{-1}).[13]

To evaluate the temperature independence of the self-temperature-compensated sensors fabricated mainly by nearly zero temperature coefficient PPy-Ag hybrid aero-sponges, the resistance responses upon the different compressive pressure at 15 and 25 °C were investigated (Figure 5f). By comparison, there was little difference of the sensing performance of the optimized PPy-Ag NW aero-sponge sensor at two temperatures with a difference of 10 °C. Furthermore, the internal-current-induced Joule heating was also considered in this work to investigate the sensing stability of the nearly zero temperature coefficient sensor by imposing a series of persistent compressive pressure (last for more than 60 s for each pressure) on the hybrid aero-sponge at ε = 5−80%. The relative electric resistance changes maintained nearly constant under each pressure stimulus (Figure 5g), confirming the temperature-independent sensing performance of the nearly zero temperature coefficient sensor from another aspect.

Additionally, although the influence of temperature on the electric conductivity has been overcome by the hybridization of Ag and PPy, the humidity or oxygen in environment is likely to affect the electricity conductivity of PPy after a long period of time. So the aero-sponges were kept in valve bag carefully to isolate

from humidity or oxygen. The electric conductivity of the obtained aero-sponge was basically stable in our experimental period. In the further application, the encapsulation of these porous sensing materials is quite necessary and vital to avoid the influence of environment.

In addition, the PPy-Ag NW aero-sponges with nearly zero temperature coefficient resistances are also expected to fabricate a promising stress-triggered Joule heater. Under compression, the electric resistance can be reduced by 83% at most, which means that the Joule heating generation can be raised by 4.88 times. Inputting a proper voltage, the thermal generation may be inconspicuous for aero-sponge in original state, while for the compressed aero-sponge the Joule heating can raise its temperature considerably, named stress-triggered Joule heating. The stress-triggered Joule heater can be fabricated by placing the electric circuit containing the PPy-Ag NW hybrid aero-sponge upon silicon dioxide (SiO_2) aerogel thermal insulating blanket and then covering it by a reversible thermo-allochroic membrane (Figure 6a, see Supporting Information Methods for thermo-allochroic membrane preparation details). Inputting a persistent voltage of 3 V for 160 s, the Joule heating generated by electric current running through the original aero-sponge was mostly dissipated by heat convection, leading to invisible differences of the thermo-allochroic membrane (Figure 6b). However, if a persistent compressive pressure was imposed on the hybrid aero-sponge, the electric current was boosted by nearly 4 times. The increased Joule heating caused by the raised current was collected effectively. Thus, the aero-sponge was warmed and induced the color changes of the thermo-allochroic membrane once temperature exceeded 43 °C (Figure 6c, Supporting Information Video S1). Once the compressive pressure was released, the temperature of the aero-sponge returned to the ambient level and the membrane recovered its color.

It is worthwhile to notice that the electric current value of the hybrid aero-sponge showed little changes while it was warmed after pressure-triggering. It means that the output power was maintained as a constant. It is because of the temperature-independent electric resistance of the aero-sponges that the steady and controlled Joule heating can be generated by adjusting the input voltage. Our future work will concentrate on creating intelligent Joule-heating blankets and 2D stress sensors. Both of the two devices will be built mainly by PPy-Ag NW aero-sponge thin films sandwiched by thermo-insulating and flexible electrodes or PPy-Ag NW aero-sponges with treated surfaces collecting electricity better. (a) For intelligent Joule-heating blankets, imposing on proper electricity inputs, it will start to generate

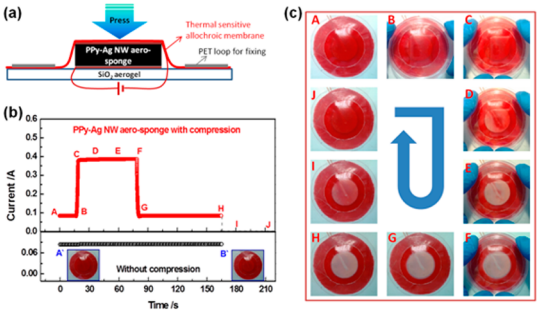

Figure 6. Fabrication process and the performance of stress-triggered Joule heater. (a) Schematic illustration on how to construct a stress-triggered Joule heater with PPy-Ag NW aero-sponge and reversible thermo-allochroic membrane. (b) Real-time *I*−*t* curves of the stress-triggered Joule heater under both natural and compressive states with 3 V voltage input, and inset is the digital pictures of the Joule heater in natural state. (c) Digital pictures of the intelligent Joule heater at the corresponding time point marked in (b).

heating at certain sites suffering compressions while it remains original temperature in natural state. The low thermo-conductivity of aero-sponges brought by the porous structure will largely avoid the energy transfer in plane so as to realize the precisely site-selected Joule-heating. (b) 2D stress sensors fabricated by PPy-Ag NW aero-sponge could potentially rival existing flexible 2D stress sensor in easy process. They will relieve people from onerous fabrication of sensing element arrays for the reason that it could be cut into any shape arbitrarily. These 2D stress sensors will detect the planar pressure distributions contributed by the electric resistance changes caused directly by the compression strains.

CONCLUSIONS

In conclusion, we have realized the programmed synthesis of conductive PPy-Ag NW hybrid aero-sponge for the first time *via* Incipient Network Conformal Growth (INCG) technology; specifically, pyrrole was polymerized *in situ* on the surface of incipient 3D networks formed by Ag NWs suspension. The microstructures of the resulting materials, such as the junction joint density and the shell thickness, can be regulated by synthetic procedure *via* changing the concentration of Ag NWs, reacting time and the feeding ratio of Py and Ag NWs. Nearly zero temperature coefficient (0.86×10^{-3}/°C) PPy-Ag NW hybrid aero-sponge can be prepared by optimizing the microstructure of the material *via* regulating the Ag NWs concentration and PPy shell thickness. The resulting aero-sponges have been processed into a piezoresistive sensor with high sensing stability (suffering more than 3000 times repeated stimuli, 10 °C temperature changes or 3 V electric heating for 160 s), high sensitivity (0.33 kPa^{-1}), short response time (1 ms) and low minimum detectable pressure (4.93 Pa). Moreover, a stress-triggered Joule heater can be also fabricated

mainly by the PPy-Ag NW hybrid aero-sponge with nearly zero temperature coefficient. Our future work will concentrate on creating intelligent Joule-heating blankets and 2D stress sensors.

METHODS

Materials. Pyrrole (98.0%), silver nitrate (99.9%), sodium chloride (99.5%), and ethylene glycol (99%) were purchased from Sinopharm Chemical Reagent Co., Ltd. Polyvinylpyrrolidone (Mw: 1 300 000, AR) were purchased from Aladdin. The water (18 MΩ cm) used in all syntheses was obtained from a milli-Q purification system. The pyrrole was distilled under reduced pressure before use. All the other chemicals were used as received without further purification.

Synthesis of Ag Nanowires. Ag nanowires (Ag NWs) were prepared by the polyol hydrothermal synthesis method,[58] described briefly as follows: 6.9 mg sodium chloride and 2.64 g polyvinylpyrrolidone were added to 90 mL ethylene glycol under 90 °C (solution 1), and 1.02 g silver nitrate was dissolved in 60 mL of ethylene glycol (solution 2). In the next, solution 2 was added dropwise to solution 1 over 30 min. Then, the mixed solution was heated at 160 °C for 6 h *via* a solvent thermal process. The product was purified by centrifugation with water and ethanol for several times.

Preparation of the PPy-Ag NW Hybrid Aero-Sponges. Ag NWs were dispersed in H_2O-ethanol (1:1 v/v) mixed solvent with a proper volume friction. Py monomer was then added into the suspension with continuous agitation. In the next, the silver nitrate (with the equimolar amounts of pyrrole) was introduced into the reactant solution rapidly as the oxidant and vigorously stirred for 30 s. The mixed solution was gelated in hours. The initial PPy-Ag NW gels were aged at room temperature for 24 h and purified *via* 7 days solvent exchange with a large amount of deionized water to remove unreacted monomer and other impurities. At last, the PPy-Ag NW gels were converted into aero-sponge by supercritical CO_2 drying process.

Characterizations. The compressive stress−strain measurements were performed on the elastic PPy-Ag NW aero-sponge by using a tensile testing machine at a crosshead speed of 5 mm/min. The electric resistance and stress sensing performance of the obtained aero-sponges were measured by real-time testing the electric current of series circuit which contained the tested samples under 1 or 3 V input voltage. Raman spectra were recorded on a LavRAM Aramis spectrometer with 50 mW He−Ne laser operating at 632.8 nm with a CCD detector. X-ray diffraction (XRD) patterns were recorded on a D8 Advance, Bruker AXS diffractometer using Cu Kα radiation (λ = 1.5406 Å) and operating at 40 kV and 40 mA. The XRD data was collected as a scanning rate of 0.04/s over an angular range of 10−80° (2θ). The morphologies of the obtained PPy-Ag NW aero-sponge were examined by SEM (Hitachi S-4800) with the acceleration voltage of 10−20 kV and Transmission Electron Microscope (TEM, Tecnai G2 F20 S-Twin) with the acceleration voltage of 200 kV. The diameter of the cross section of gel skeleton were measured and analyzed with Image-Pro Plus (IPP) software.

Conflict of Interest: The authors declare no competing financial interest.

Acknowledgment. This work was financially supported by the National Natural Science Foundation of China (21373024, 21404117), the Natural Science Foundation of Jiangsu Province (BK20140391), the 100 Talents Program of the Chinese Academy of Sciences, the Innovation Program of the Beijing Institute of Technology and the Postdoctoral Research Foundation of Jiangsu Province (1401066C) for financial support.

Supporting Information Available: Experiments (including synthesis and characterization), theoretical analysis methods, additional figures (including SEM pictures, spectra and electric resistance detections), tables summarizing the statistics data of shell diameters and a supplementary video for stress-triggered Joule heating. This material is available free of charge *via* the Internet at http://pubs.acs.org.

REFERENCES AND NOTES

1. Huang, X.; Tan, C.; Yin, Z.; Zhang, H. 25th Anniversary Article: Hybrid Nanostructures Based on Two-Dimensional Nanomaterials. *Adv. Mater.* **2014**, *26*, 2185–2204.
2. Andrews, M. B.; Cahill, C. L. Uranyl Bearing Hybrid Materials: Synthesis, Speciation, and Solid-State Structures. *Chem. Rev.* **2013**, *113*, 1121–1136.
3. Feng, J.; Zhang, H. Hybrid Materials Based on Lanthanide Organic Complexes: A Review. *Chem. Soc. Rev.* **2013**, *42*, 387–410.
4. Liang, Y.; Li, Y.; Wang, H.; Dai, H. Strongly Coupled Inorganic/Nanocarbon Hybrid Materials for Advanced Electrocatalysis. *J. Am. Chem. Soc.* **2013**, *135*, 2013–2036.
5. Yu, G.; Xie, X.; Pan, L.; Bao, Z.; Cui, Y. Hybrid Nanostructured Materials for High-Performance Electrochemical Capacitors. *Nano Energy* **2013**, *2*, 213–234.
6. Noh, J. H.; Im, S. H.; Heo, J. H.; Mandal, T. N.; Seok, S. I. Chemical Management for Colorful, Efficient, and Stable Inorganic-Organic Hybrid Nanostructured Solar Cells. *Nano Lett.* **2013**, *13*, 1764–1769.
7. Peng, L.; Peng, X.; Liu, B.; Wu, C.; Xie, Y.; Yu, G. Ultrathin Two-Dimensional MnO_2/Graphene Hybrid Nanostructures for High-Performance, Flexible Planar Supercapacitors. *Nano Lett.* **2013**, *13*, 2151–2157.
8. Jeon, N. J.; Noh, J. H.; Kim, Y. C.; Yang, W. S.; Ryu, S.; Seok, S. I. Solvent Engineering for High-Performance Inorganic-Organic Hybrid Perovskite Solar Cells. *Nat. Mater.* **2014**, *13*, 897–903.
9. Luo, S.; Liu, T. SWCNT/Graphite Nanoplatelet Hybrid Thin Films for Self-Temperature-Compensated, Highly Sensitive, and Extensible Piezoresistive Sensors. *Adv. Mater.* **2013**, *25*, 5650–5657.
10. Yamada, T.; Hayamizu, Y.; Yamamoto, Y.; Yomogida, Y.; Izadi-Najafabadi, A.; Futaba, D. N.; Hata, K. A Stretchable Carbon Nanotube Strain Sensor for Human-Motion Detection. *Nat. Nanotechnol.* **2011**, *6*, 296–301.
11. Park, J.; Lee, Y.; Hong, J.; Ha, M.; Jung, Y.-D.; Lim, H.; Kim, S. Y.; Ko, H. Giant Tunneling Piezoresistance of Composite Elastomers with Interlocked Microdome Arrays for Ultrasensitive and Multimodal Electronic Skins. *ACS Nano* **2014**, *8*, 4689–4697.
12. Wang, X.; Gu, Y.; Xiong, Z.; Cui, Z.; Zhang, T. Silk-Molded Flexible, Ultrasensitive, and Highly Stable Electronic Skin for Monitoring Human Physiological Signals. *Adv. Mater.* **2014**, *26*, 1336–1342.
13. Yao, H. B.; Ge, J.; Wang, C. F.; Wang, X.; Hu, W.; Zheng, Z. J.; Ni, Y.; Yu, S. H. A Flexible and Highly Pressure-Sensitive Graphene-Polyurethane Sponge Based on Fractured Microstructure Design. *Adv. Mater.* **2013**, *25*, 6692–6698.
14. Choong, C. L.; Shim, M. B.; Lee, B. S.; Jeon, S.; Ko, D. S.; Kang, T. H.; Bae, J.; Lee, S. H.; Byun, K. E.; Im, J.; et al. Highly Stretchable Resistive Pressure Sensors Using a Conductive Elastomeric Composite on a Micropyramid Array. *Adv. Mater.* **2014**, *26*, 3451–3458.
15. Hou, C.; Wang, H.; Zhang, Q.; Li, Y.; Zhu, M. Highly Conductive, Flexible, and Compressible All-Graphene Passive Electronic Skin for Sensing Human Touch. *Adv. Mater.* **2014**, *26*, 5018–5024.
16. Tien, N. T.; Jeon, S.; Kim, D. I.; Trung, T. Q.; Jang, M.; Hwang, B. U.; Byun, K. E.; Bae, J.; Lee, E.; Tok, J. B.; et al. A Flexible Bimodal Sensor Array for Simultaneous Sensing of Pressure and Temperature. *Adv. Mater.* **2014**, *26*, 796–804.
17. Zeng, W.; Shu, L.; Li, Q.; Chen, S.; Wang, F.; Tao, X. M. Fiber-Based Wearable Electronics: A Review of Materials, Fabrication, Devices, and Applications. *Adv. Mater.* **2014**, *26*, 5310–5336.
18. Brady, S.; Diamond, D.; Lau, K.-T. Inherently Conducting Polymer Modified Polyurethane Smart Foam for Pressure Sensing. *Sens. Actuators, A* **2005**, *119*, 398–404.

19. Park, S.; Kim, H.; Vosgueritchian, M.; Cheon, S.; Kim, H.; Koo, J. H.; Kim, T. R.; Lee, S.; Schwartz, G.; Chang, H.; et al. Stretchable Energy-Harvesting Tactile Electronic Skin Capable of Differentiating Multiple Mechanical Stimuli Modes. *Adv. Mater.* **2014**, *26*, 7324–7332.
20. Akbar, M.; Shanblatt, M. A. Temperature Compensation of Piezoresistive Pressure Sensors. *Sens. Actuators, A* **1992**, *33*, 155–162.
21. Gakkestad, J.; Ohlckers, P.; Halbo, L. Compensation of Sensitivity Shift in Piezoresistive Pressure Sensors Using Linear Voltage Excitation. *Sens. Actuators, A* **1995**, *49*, 11–15.
22. Wang, Q.; Ding, J. N.; Wang, W. X. Fabrication and Temperature Coefficient Compensation Technology of Low Cost High Temperature Pressure Sensor. *Sens. Actuators, A* **2005**, *120*, 468–473.
23. Han, J. Q.; Wang, X. F.; Yan, T. H.; Li, Y.; Song, M. X. A Novel Method of Temperature Compensation for Piezoresistive Microcantilever-Based Sensors. *Rev. Sci. Instrum.* **2012**, *83*, 035002.
24. Zhou, G. W.; Zhao, Y. L.; Guo, F. F.; Xu, W. J. A Smart High Accuracy Silicon Piezoresistive Pressure Sensor Temperature Compensation System. *Sensors* **2014**, *14*, 12174–12190.
25. Tappan, B. C.; Huynh, M. H.; Hiskey, M. A.; Chavez, D. E.; Luther, E. P.; Mang, J. T.; Son, S. F. Ultralow-Density Nanostructured Metal Foams: Combustion Synthesis, Morphology, and Composition. *J. Am. Chem. Soc.* **2006**, *128*, 6589–6594.
26. Nyce, G. W.; Hayes, J. R.; Hamza, A. V.; Satcher, J. H. Synthesis and Characterization of Hierarchical Porous Gold Materials. *Chem. Mater.* **2007**, *19*, 344–346.
27. Bao, Z.; Ernst, E. M.; Yoo, S.; Sandhage, K. H. Syntheses of Porous Self-Supporting Metal-Nanoparticle Assemblies with 3D Morphologies Inherited from Biosilica Templates (Diatom Frustules). *Adv. Mater.* **2009**, *21*, 474–478.
28. Tappan, B. C.; Steiner, S. A.; Luther, E. P. Nanoporous Metal Foams. *Angew. Chem., Int. Ed.* **2010**, *49*, 4544–4565.
29. Gao, D.; Yang, G.; Zhu, Z.; Zhang, J.; Yang, Z.; Zhang, Z.; Xue, D. One-Step Synthesis of Open-Cell Ni Foams by Annealing the Ni^{2+}-Based Precursor in Air. *J. Mater. Chem.* **2012**, *22*, 9462–9465.
30. Dumee, L. F.; He, L.; Lin, B.; Ailloux, F.-M.; Lemoine, J.-B.; Velleman, L.; She, F.; Duke, M. C.; Orbell, J. D.; Erskine, G.; et al. The Fabrication and Surface Functionalization of Porous Metal Frameworks—A Review. *J. Mater. Chem. A* **2013**, *1*, 15185–15206.
31. Fu, R.; Zheng, B.; Liu, J.; Dresselhaus, M. S.; Dresselhaus, G.; Satcher, J. H.; Baumann, T. F. The Fabrication and Characterization of Carbon Aerogels by Gelation and Supercritical Drying in Isopropanol. *Adv. Funct. Mater.* **2003**, *13*, 558–562.
32. Yoshizawa, N.; Hatori, H.; Soneda, Y.; Hanzawa, Y.; Kaneko, K.; Dresselhaus, M. S. Structure and Electrochemical Properties of Carbon Aerogels Polymerized in the Presence of Cu^{2+}. *J. Non-Cryst. Solids* **2003**, *330*, 99–105.
33. Moreno-Castilla, C.; Maldonado-Hódar, F. J. Carbon Aerogels for Catalysis Applications: An Overview. *Carbon* **2005**, *43*, 455–465.
34. Antonietti, M.; Fechler, N.; Fellinger, T.-P. Carbon Aerogels and Monoliths: Control of Porosity and Nanoarchitecture *via* Sol–Gel routes. *Chem. Mater.* **2014**, *26*, 196–210.
35. Zou, J.; Liu, J.; Karakoti, A. S.; Kumar, A.; Joung, D.; Li, Q.; Khondaker, S. I.; Seal, S.; Zhai, L. Ultralight Multiwalled Carbon Nanotube Aerogel. *ACS Nano* **2010**, *4*, 7293–7302.
36. Gui, X.; Wei, J.; Wang, K.; Cao, A.; Zhu, H.; Jia, Y.; Shu, Q.; Wu, D. Carbon Nanotube Sponges. *Adv. Mater.* **2010**, *22*, 617–621.
37. Bordjiba, T.; Mohamedi, M.; Dao, L. H. New Class of Carbon-Nanotube Aerogel Electrodes for Electrochemical Power Sources. *Adv. Mater.* **2008**, *20*, 815–819.
38. Bryning, M. B.; Milkie, D. E.; Islam, M. F.; Hough, L. A.; Kikkawa, J. M.; Yodh, A. G. Carbon Nanotube Aerogels. *Adv. Mater.* **2007**, *19*, 661–664.
39. Hu, H.; Zhao, Z.; Wan, W.; Gogotsi, Y.; Qiu, J. Ultralight and Highly Compressible Graphene Aerogels. *Adv. Mater.* **2013**, *25*, 2219–2223.
40. Xu, Z.; Zhang, Y.; Li, P.; Gao, C. Strong, Conductive, Lightweight, Neat Graphene Aerogel Fibers with Aligned Pores. *ACS Nano* **2012**, *6*, 7103–7113.
41. Wu, Z.-S.; Yang, S.; Sun, Y.; Parvez, K.; Feng, X.; Müllen, K. 3D Nitrogen-Doped Graphene Aerogel-Supported Fe_3O_4 Nanoparticles as Efficient Electrocatalysts for the Oxygen Reduction Reaction. *J. Am. Chem. Soc.* **2012**, *134*, 9082–9085.
42. Wu, X.; Zhou, J.; Xing, W.; Wang, G.; Cui, H.; Zhuo, S.; Xue, Q.; Yan, Z.; Qiao, S. Z. High-Rate Capacitive Performance of Graphene Aerogel with a Superhigh C/O Molar Ratio. *J. Mater. Chem.* **2012**, *22*, 23186–23193.
43. Sui, Z.; Meng, Q.; Zhang, X.; Ma, R.; Cao, B. Green Synthesis of Carbon Nanotube-Graphene Hybrid Aerogels and Their Use as Versatile Agents for Water Purification. *J. Mater. Chem.* **2012**, *22*, 8767–8771.
44. Qiu, L.; Liu, J. Z.; Chang, S. L. Y.; Wu, Y.; Li, D. Biomimetic Superelastic Graphene-Based Cellular Monoliths. *Nat. Commun.* **2012**, *3*, 1241.
45. Chen, L.; Wang, X.; Zhang, X.; Zhang, H. 3D Porous and Redox-Active Prussian Blue-in-Graphene Aerogels for Highly Efficient Electrochemical Detection of H_2O_2. *J. Mater. Chem.* **2012**, *22*, 22090–22096.
46. Zhang, X.; Sui, Z.; Xu, B.; Yue, S.; Luo, Y.; Zhan, W.; Liu, B. Mechanically Strong and Highly Conductive Graphene Aerogel and Its Use as Electrodes for Electrochemical Power Sources. *J. Mater. Chem.* **2011**, *21*, 6494–6497.
47. Sui, Z.; Zhang, X.; Lei, Y.; Luo, Y. Easy and Green Synthesis of Reduced Graphite Oxide-Based Hydrogels. *Carbon* **2011**, *49*, 4314–4321.
48. Chen, W.; Yan, L. *In situ* Self-Assembly of Mild Chemical Reduction Graphene for Three-Dimensional Architectures. *Nanoscale* **2011**, *3*, 3132–3137.
49. Xu, Y.; Sheng, K.; Li, C.; Shi, G. Self-Assembled Graphene Hydrogel *via* a One-Step Hydrothermal Process. *ACS Nano* **2010**, *4*, 4324–4330.
50. Doi, M.; Edward, S. F. *The Theory of Polymer Dynamics*; Oxford University Press: New York, 1986; pp 324–326.
51. Jung, S. M.; Jung, H. Y.; Dresselhaus, M. S.; Jung, Y. J.; Kong, J. A Facile Route for 3D Aerogels from Nanostructured 1D and 2D Materials. *Sci. Rep.* **2012**, *2*, 849.
52. Campion, A.; Kambhampati, P. Surface-Enhanced Raman Scattering. *Chem. Soc. Rev.* **1998**, *27*, 241–250.
53. Lu, Y.; He, W.; Cao, T.; Guo, H.; Zhang, Y.; Li, Q.; Shao, Z.; Cui, Y.; Zhang, X. Elastic, Conductive, Polymeric Hydrogels and Sponges. *Sci. Rep.* **2014**, *4*, 5792.
54. Ilić, D.; Butorac, J.; Ferković, L. Temperature Measurements by Means of NTC Resistors and a Two-Parameter Approximation Curve. *Measurement* **2008**, *41*, 294–299.
55. Yu, S. H.; Choi, M. S.; Yoo, P. J.; Park, J. H.; Park, J. H.; Cho, J. H.; Chung, G. S.; Lee, J. Y. Temperature Sensing Behavior of Poly(3,4-ethylenedioxythiophene) Thin Film. *Synth. Met.* **2013**, *185–186*, 52–55.
56. Pan, L.; Chortos, A.; Yu, G.; Wang, Y.; Isaacson, S.; Allen, R.; Shi, Y.; Dauskardt, R.; Bao, Z. An Ultra-Sensitive Resistive Pressure Sensor Based on Hollow-Sphere Microstructure Induced Elasticity in Conducting Polymer Film. *Nat. Commun.* **2014**, *5*, 3002.
57. Pang, C.; Lee, G.-Y.; Kim, T.-i.; Kim, S. M.; Kim, H. N.; Ahn, S.-H.; Suh, K.-Y. A Flexible and Highly Sensitive Strain-Gauge Sensor Using Reversible Interlocking of Nanofibres. *Nat. Mater.* **2012**, *11*, 795–801.
58. Sun, Y. G.; Mayers, B.; Herricks, T.; Xia, Y. N. Polyol Synthesis of Uniform Silver Nanowires: A Plausible Growth Mechanism and the Supporting Evidence. *Nano Lett.* **2003**, *3*, 955–960.